Journal of Materials Chemistry C

Accepted Manuscript

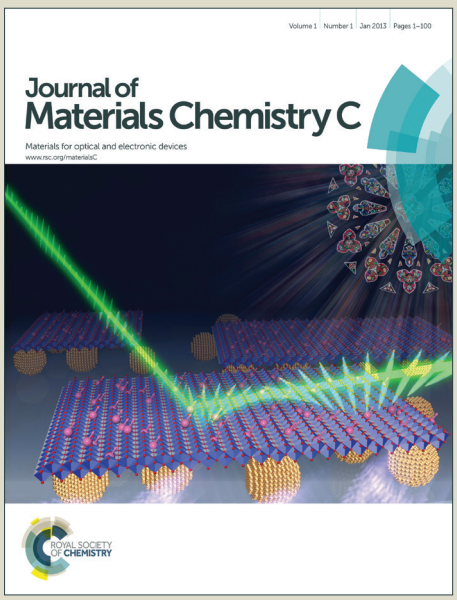

ROYAL SOCIETY OF CHEMISTRY

www.rsc.org/materialsC

Enhanced magnetodielectric interaction of (1-x)$BaTiO_3$-x$CoFe_2O_4$ multiferroic composites

Yajing Shen,[1] Junpeng Sun,[2] Linglong Li,[1] Yonggang Yao,[1] Chao Zhou,[1] Ran Su,[1] Yaodong Yang[1,a)]

A simplified one-pot solid-state reaction is developed to synthesize (1-x)$BaTiO_3$-x$CoFe_2O_4$ composites, which can enhance the magnetodielectric interaction between different phases.

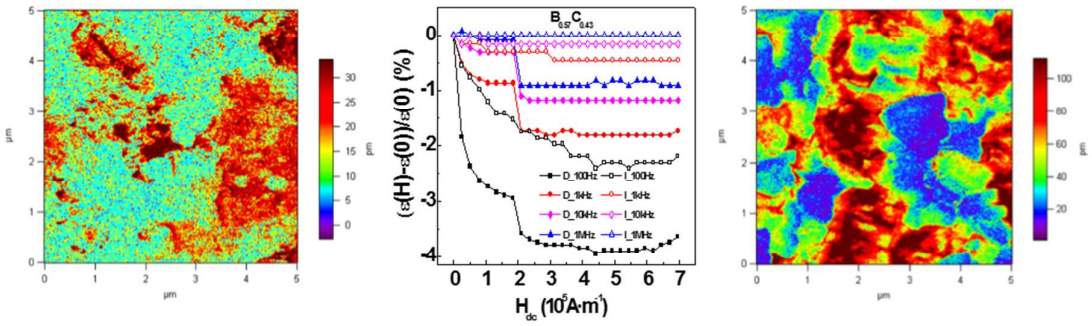

Journal Name Journal of Materials Chemistry C RSCPublishing

ARTICLE

Enhanced magnetodielectric interaction of (1-x)$BaTiO_3$-x$CoFe_2O_4$ multiferroic composites

Cite this: DOI: 10.1039/xoxxoooooox

Received ooth xxxxxxxxx 20xx,
Accepted ooth xxxxxxxxx 20xx

DOI: 10.1039/xoxxoooooox

www.rsc.org/

Yajing Shen,[1] Junpeng Sun,[2] Linglong Li,[1] Yonggang Yao,[1] Chao Zhou,[1] Ran Su,[1] Yaodong Yang[1,a)]

[1] Multi-disciplinary Materials Research Center, Frontier Institute of Science and Technology, Xi'an Jiaotong University, Xi'an 710049, China
[2] State Key Lab of Electrical Insulation and Power Equipment, Xi'an Jiaotong University, Xi'an 710049, China
[a)] yaodongy@mail.xjtu.edu.cn

Multiferroic composites containing barium titanate ($BaTiO_3$) and cobalt ferrite ($CoFe_2O_4$) were synthesized by a simplified one pot solid-state reaction process in which all basic chemicals ($BaCO_3$, TiO_2, Fe_2O_3, CoO) were directly mixed together. Compared with conventional two steps solid-state reaction process, the simplified process tends to form smaller grains, and enhance the magnetodielectric interaction between different phases, which will indirectly benefit the magnetoelctric coupling.

1 Introduction

Multiferroic materials, which simultaneously exhibit ferroelectricity, ferromagnetism and unique product tensor property: magnetoelectric (ME) effect, have drawn much interest due to their potential applications in multifunctional devices such as transducers, actuators, and sensors.[1-7] In these multiferroic materials, the ME effect results from the coupling interaction between multiferroic orders, including the direct ME effect (i.e., an electric polarization or electric field appears upon an applied magnetic field) and reverse ME effect (i.e., a magnetization is induced by an applied electric field).[8] Very few single phase multiferroic materials exist in nature or have been synthesized in the laboratory,[9-11] their ME effect generally occurs at a very low temperature (multiferroic property of $Ni_3B_7O_{13}I$ appears at 46K),[12] and is too weak to be used in practical applications.[8, 13] On the contrary, the multiferroic composites consisting of piezoelectric and magnetostrictive phases show an appreciable ME effect at a very wide temperature range,[14] and the ME effect in composites is induced by the strain transfer between two phases.[15-17]

So far, multiferroic composites with various connectivity schemes and different scales have been synthesized by various chemical and physical methods.[18-24] Unidirectional solidification of the quinary system Fe-Co-Ti-Ba-O,[25-27] solid-state reaction method,[28-32] pulsed laser deposition,[20, 33-38] sol-gel method,[39-43] and electrospinning[21, 44, 45] are some main synthesis methods. Unfortunately, unidirectional solidification is complex and costing: it not only involves careful control over the cooling rate and temperature, but also requires critical control on the composition. Due to different nucleation and growth rates of each individual phase, the pulsed laser deposition method also involves complex synthesis process, while facing a high cost with a limited yield problem. Sol-gel spin coating and electrospinning, two low cost methods, yet have an obvious disadvantage: organometallic precursors are used in these processes, which will result in many environmental concerns.

Compared with above four synthesis methods, the conventional solid-state reaction method has many advantages. It is not only a low cost and an easy handling method, but also enables a large yield without seriously environmental problems. But the conventional solid-state reaction route is somewhat cumbersome. It requires two steps: firstly, the individual piezoelectric phase and magnetostrictive phase are prepared by standard ceramic method, respectively; secondly, these piezoelectric and magnetostrictive powders are mixed and sintered again to obtain final multiferroic composites. In this case, the thermal expansion mismatch between two phases leads to a poor interfacial connection, and goes against the strain transferring from one phase to another, which limits the ME interaction.[46, 47] The question is if we can merge two steps into a one pot reaction to simplify the synthesis process?

In this study, inspired by Yang et al.'s synthesis method,[48] the conventional solid-state reaction process was simplified to a one step route by directly mixing all basic oxide chemicals in one pot. $BaTiO_3$-$CoFe_2O_4$ is a widely investigated multiferroic composite, and its ME coefficient is in a wide range from 0.19 to 180mV·cm^{-1}·Oe^{-1},[49-52] depending on preparation methods, and the microstructures. Here, we selected this typical ME

composite as our exemplary product to develop the one pot reaction. Their crystal structure, morphology, magnetic, piezoelectric properties were investigated and also compared with these samples obtained under the similar control conditions via conventional two steps solid-state reaction route.

2 Experiment

Two groups of (1-x)$BaTiO_3$-x$CoFe_2O_4$ or $B_{1-x}C_x$ composites were fabricated by the simplified and conventional solid-state reactions, respectively. In the simplified solid-state reaction route, all four basic chemicals ($BaCO_3$, TiO_2, Fe_2O_3, CoO) were directly mixed together at suitable stoichiometric proportions in a ball mill for 6h. The powders were calcined for 5h in air at 850℃ for solid-state reaction to synthesize (1-x)$BaTiO_3$-x$CoFe_2O_4$ composite powders in one step. The as-obtained powders were pressed into disk shape and sintered in air for 5h at 1000℃. This group of samples was marked as D-group (direct reaction group). Whereas I-group samples (indirect reaction group, this group of samples were fabricated by the conventional solid-state reaction route) were obtained via two steps. Firstly, the individual $BaTiO_3$ and $CoFe_2O_4$ powders were synthesized separately by a standard ceramic method. The $BaTiO_3$ and $CoFe_2O_4$ powders both were calcined for 5h in air at 850℃. Secondly, these as-prepared $BaTiO_3$ and $CoFe_2O_4$ powders were mixed together in suitable proportions in a ball mill for 6h. The mixed powders were pressed into disk shape and sintered in air for 5h at 1000℃.

Structural analysis was performed by X-ray diffractometer (XRD, Shimadzu 7000). The patterns were recorded in a 2theta range from 20° to 80° with a step of 2°/min. The morphology was observed by a scanning electron microscope (SEM, Quanta F250), and the corresponding grain size was calculated by Nano Measurer 1.2 software. The magnetic hysteresis loops were measured by a vibrating sample magnetometer (VSM-7307, Lakeshore). The piezoelectric properties were investigated by an atomic force microscope (AFM, Cypher, Asylum Research). The temperature dependent magnetization measurement was carried out by VSM module of a physics property measurement system (PPMS, Quantum Design) in the temperature range from 350K to 150K with a cooling rate of 2K/min under a constant magnetic field of 79600A·m^{-1}. Sensitivity of PPMS-VSM is 2*10^{-11}A·m^2 and stability of temperature control is ± 0.02%. Magnetodielectric (MD), the relative dielectric permittivity change as a function of an applied magnetic field strength, was measured by combining a HIOKI LCR meter into the VSM-7307.

3 Results and discussion

Fig. 1 shows the X-ray diffraction patterns of $BaTiO_3$-$CoFe_2O_4$ composites fabricated by different processes. Individual $BaTiO_3$ (perovskite structure) and $CoFe_2O_4$ (spinel structure) are also listed here as references. For all the samples, the X-ray diffraction patterns show a mixture of two clear phases (perovskite and spinel structures), indicating that the multiferroic composites containing piezoelectric and magnetostrictive phases were synthesized by both routes. With molar fraction of $CoFe_2O_4$ increasing, the intensity of $CoFe_2O_4$ peaks increases in both groups. The XRD data of two groups is totally consistent at both the angle position and intensity of all peaks at a same composition. There are a few additional minor peaks in the composites. Minor peaks at 32.1°, 33.2°, 34.1°, 40.3°, 49.5°, 54°, 64° are well indexed as the Fe_2O_3 peaks, while the one at 42.5° is CoO peak, indicating that there is a little residual Fe_2O_3 and CoO from raw materials in both groups samples.

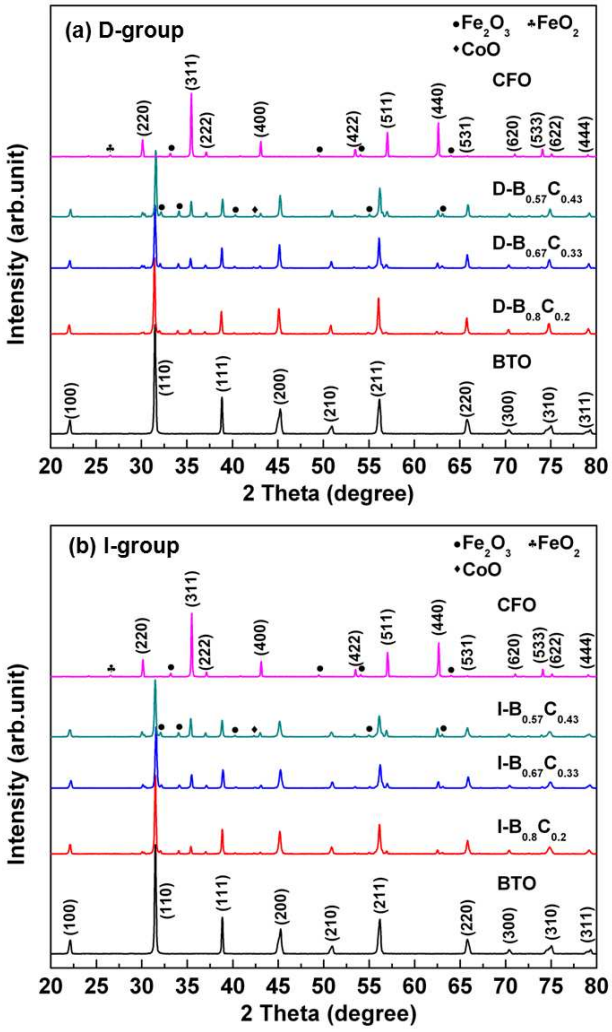

Fig. 1 X-ray diffraction patterns of $BaTiO_3$, $CoFe_2O_4$, and (1-x)$BaTiO_3$-x$CoFe_2O_4$ (x is molar fraction of $CoFe_2O_4$) composites: (a) D-group, (b) I-group.

Fig. 2 are the SEM images to show the morphology of two groups of composites. Images in the left (right) column illustrate how the grain geometry varies with composition change for D-group (I-group). Individual $BaTiO_3$ and $CoFe_2O_4$ are listed at fig. 2(g) and fig. 2(h) as references. For D-group samples, some grains in D-$B_{0.8}C_{0.2}$ have triangle faces. Whereas with the molar fraction of $CoFe_2O_4$ increasing, grains in D-$B_{0.67}C_{0.33}$ and D-$B_{0.57}C_{0.43}$ samples become more irregular. By contrast, some grains of I-$B_{0.8}C_{0.2}$ sample show typical octahedral morphology with four faces on each hemisphere, whereas grains in I-$B_{0.67}C_{0.33}$ sample show octahedral-like morphology too, more obvious chamfering can be found in I-$B_{0.57}C_{0.43}$ sample.

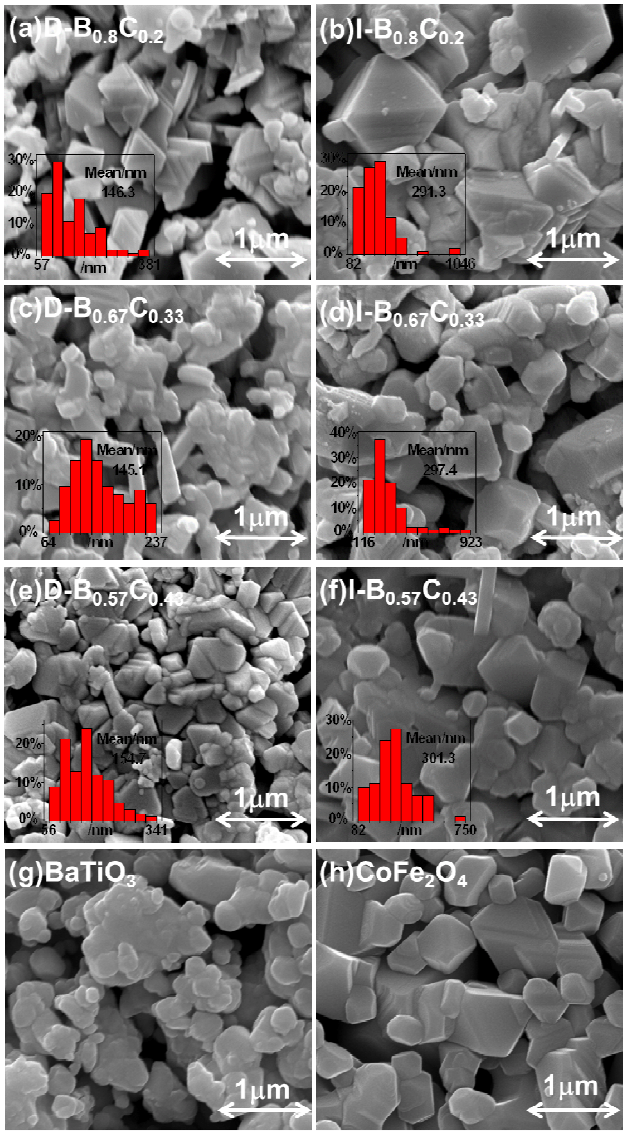

Fig. 2 Scanning electron microscope images of different samples: (a) D-$B_{0.8}C_{0.2}$, (b) I-$B_{0.8}C_{0.2}$, (c) D-$B_{0.67}C_{0.33}$, (d) I-$B_{0.67}C_{0.33}$, (e) D-$B_{0.57}C_{0.43}$, (f) I-$B_{0.57}C_{0.43}$, (g) $BaTiO_3$, and (h) $CoFe_2O_4$. The insets show their statistical distributions of grain size and highlight the average grain sizes.

By comparing these images between D-group and I-group, it can be seen that I-group samples contain clear octahedral-like grains corresponding to $CoFe_2O_4$ spinel structure; whereas only some irregular grains in D-group samples. The insets are the statistical distributions of grain size and highlight their average grain sizes (measured by Nano Measurer 1.2 software). From the insets, it is noticed that the average grain sizes of D-$B_{0.8}C_{0.2}$, D-$B_{0.67}C_{0.33}$, and D-$B_{0.57}C_{0.43}$ are 146.3nm, 145.1nm, 154.7nm, respectively, half smaller than those of I-$B_{0.8}C_{0.2}$ (291.3nm), I-$B_{0.67}C_{0.33}$ (297.4nm), and I-$B_{0.57}C_{0.43}$ (301.3nm) samples. The diverse average grain sizes as well as morphologies result from the different reaction routes. For D-group, all four basic chemicals ($BaCO_3$, TiO_2, Fe_2O_3, CoO) were mixed rather homogeneous, the $BaTiO_3$ perovskite structure and $CoFe_2O_4$ spinel structure turn out to grow at the same time in one calcining process, resulting in the small grain size and irregular morphology. Whereas in I-group, the $BaTiO_3$ and $CoFe_2O_4$ powders were synthesized separately, so the corresponding perovskite and spinel structures can grow freely, leading to bigger grain size. After these $BaTiO_3$ and $CoFe_2O_4$ powders are mechanically mixed together for sintering, two phases are relatively independent, and their average grain sizes remain unchanged.

The magnetic hysteresis loops of all samples are shown in fig. 3. Here the magnetization was already normalized by the mass of $CoFe_2O_4$ in different composites. From fig. 3, it can be noticed that the saturation magnetization of individual $CoFe_2O_4$ is the highest, reaching 72A·m^2·kg^{-1}. When mixed with $BaTiO_3$, its saturation magnetization decreases with the molar fraction of $BaTiO_3$ increases. This phenomenon originates from that the mixed $BaTiO_3$ phase acts as non-magnetic defects, first hindering the growth of magnetic domains in $CoFe_2O_4$ and also hindering the movement of magnetic domains in $CoFe_2O_4$ under an external field. These effects will result in small magnetic domains, which are difficult to make one totally consistent orientation.

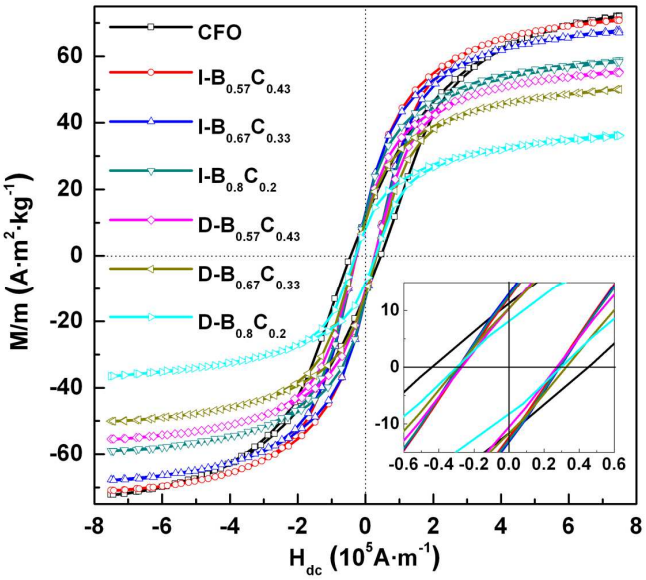

Fig. 3 Magnetic hysteresis loops of $CoFe_2O_4$ and (1-x)$BaTiO_3$-x$CoFe_2O_4$ composites measured at room temperature. The inset is the enlarged center area.

However, one can still notice that D-group and I-group have distinctly different magnetization change tendencies with $BaTiO_3$ content increasing. The saturation magnetization of D-group decreases much faster than that of I-group, suggesting that there is stronger interaction between $BaTiO_3$ and $CoFe_2O_4$ in D-group than I-group.

The piezoelectric properties of D-group were investigated by piezoresponse force microscope (PFM), and compared to those of I-group at a same composition: i.e. $B_{0.57}C_{0.43}$. Similar results were also found in other compositions. Fig. 4 shows the PFM images of D-$B_{0.57}C_{0.43}$ and I-$B_{0.57}C_{0.43}$ samples. From the height data (fig. 4a and fig. 4e), it can be noticed that the grain size of D-$B_{0.57}C_{0.43}$ sample is much smaller than that of I-$B_{0.57}C_{0.43}$ sample, which is consistent with the SEM results. The distinct contrast on different grains can be observed in the amplitude data (fig. 4b and fig. 4f) to distinguish the magnetostrictive

$CoFe_2O_4$ from the piezoelectric $BaTiO_3$. The brown part where has higher piezoresponse is piezoelectric $BaTiO_3$ phase, and the blue part where has almost no signal is magnetostrictive $CoFe_2O_4$ phase. Clear, fig. 4f is much more colourful than fig. 4b and there are obvious interfaces between $BaTiO_3$ phase and $CoFe_2O_4$ phase in I-$B_{0.57}C_{0.43}$ sample (fig.4f), while those interfaces are blurry in D-$B_{0.57}C_{0.43}$ sample. Again, it indicates that the interfacial connection of two phases in D-$B_{0.57}C_{0.43}$ sample is tighter. The phase data (fig. 4c and fig. 4g) correspond very well with the amplitude data (fig. 4b and fig. 4f), revealing ferroelectric domain patterns at $BaTiO_3$ piezoelectric phase region only.

Fig. 4d and fig. 4h show the different amplitude-voltage curves from both samples, measurement locations are marked in fig. 4c and fig. 4g. The switching PFM measurement was actually carried out at many different locations for each sample, and they all showed similar results, we only show one example here. Larger switching voltage (30V) as well as obviously restrained amplitude-voltage loop is observed in D-$B_{0.57}C_{0.43}$ sample, while the switching voltage for I-$B_{0.57}C_{0.43}$ sample is only 5V.

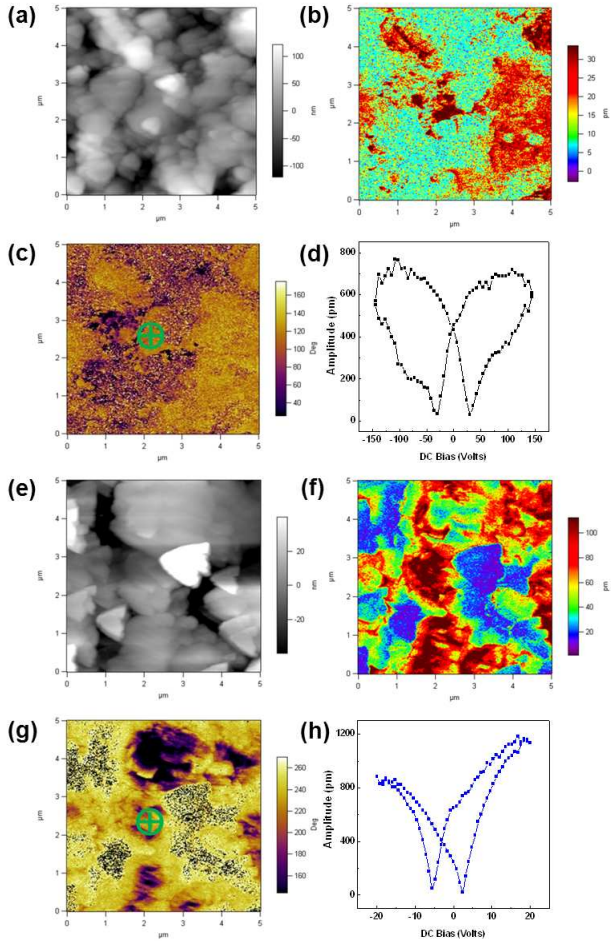

Fig. 4 Piezoresponse force microscope images of D-$B_{0.57}C_{0.43}$ (a, b, c, d) and I-$B_{0.57}C_{0.43}$ (e, f, g, h): (a and e) height images, (b and f) amplitude images, (c and g) phase images, (d and h) amplitude-voltage curves.

To further understand the interaction between $BaTiO_3$ and $CoFe_2O_4$, the temperature dependent magnetization measurement was carried out on both groups under an applied magnetic field (79600A·m^{-1}, larger than the coercive fields of all samples) during cooling process. Fig. 5 shows the temperature dependence of magnetization and its first order differential over temperature (d(M/m)/dT) curves of these composites. When cooling from 350K to 150K, the magnetization of all samples keeps increasing, but their changing tendencies are different. The difference is illustrated by the corresponding first order differential curves of magnetization over temperature.

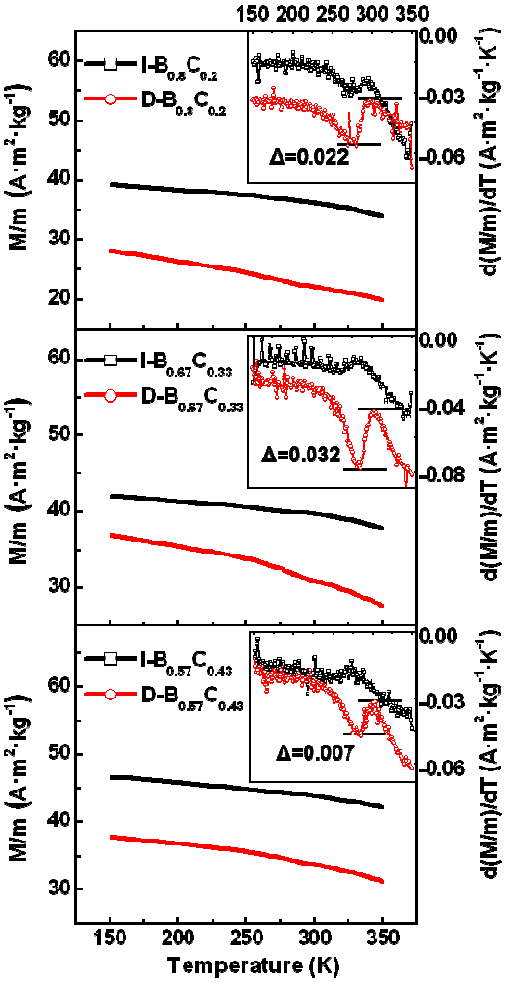

Fig. 5 Temperature dependence of magnetization (at 79600A·m^{-1}) and its first order differential over temperature (d(M/m)/dT) curves of (1-x)$BaTiO_3$-x$CoFe_2O_4$ composites from different fabrication processes.

When the temperature decreases to the phase transition point of $BaTiO_3$ (at 275K, from tetragonal phase to orthorhombic phase), two obvious inflection points occur in the temperature dependent magnetization curves successively, corresponding to the peak and drop of the first order differential curves. The anomaly of magnetization increase tendency originates from the structure change of $BaTiO_3$ at 275K. When the crystal structure of $BaTiO_3$ evolves from tetragonal phase to orthorhombic phase, the product strain transfers from the

$BaTiO_3$ to magnetostrictive $CoFe_2O_4$ through the interfaces, further affecting the magnetization of $CoFe_2O_4$. Seen from the insets of first order differential curves of magnetization over temperature, the influence of structure change of $BaTiO_3$ on magnetization of $CoFe_2O_4$ is much bigger in D-group than I-group.

We also measured magnetodielectric (MD) properties of our composites, which can exhibit the ME effect from another aspect. Jang et al. used this method to study the ME coupling in La-doped BFO films;[53] M. P. Singh et al. studied the magnetocapacitance effect of $La_{0.7}Ca_{0.3}MnO_3/BaTiO_3$ perovskite-superlattices;[54] I. Fina et al. investigated the ME coupling of $BaTiO_3$-$CoFe_2O_4$ nanocomposite thin films by magnetocapacitance measurements too.[55] Here, fig. 6 presents the change in the real part of relative dielectric permittivity of the (1-x)$BaTiO_3$-x$CoFe_2O_4$ composites as a function of magnetic field H at room-temperature. Clearly, the capacitance is decreasing under a magnetic field. Below a certain critical probing frequency (10kHz), curves also show a clearly frequency-dependent MD response: with increasing frequency, MD susceptibility (the slope of curves in fig. 6) decreases; whereas higher than the critical value, the MD effect is found to be essentially independent of the probing frequency. The MD effect at a low-frequency region (f＜10kHz) can be attributed to the magnetoresistance effect combined with the Maxwell-Wagner effect.[56] In our composite case, the significant contribution can come from both phases and the interaction between them. At the low-frequency region (f＜10kHz), a dramatically enhanced MD change is observed in D-group, which originates from its smaller grain size and tighter interfacial connection.

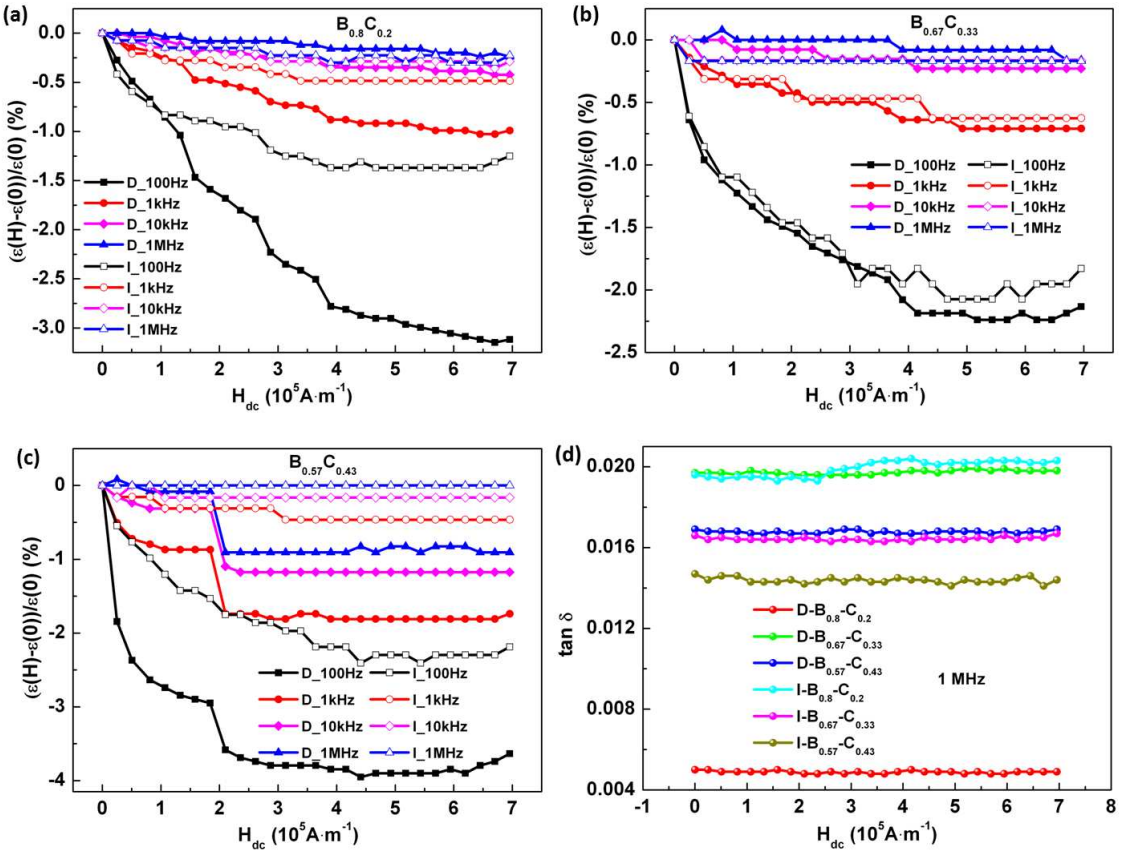

Fig. 6 MD responses of the (1-x)$BaTiO_3$-x$CoFe_2O_4$ composites at various frequencies. (a) $B_{0.8}C_{0.2}$, (b) $B_{0.67}C_{0.33}$ and (c) $B_{0.57}C_{0.43}$. (d) Tangent loss (magnetoloss) as a function of H at a frequency of 1MHz.

After eliminating the interference from other effects, MD changes detected above 10kHz can be used to evaluate the intrinsic ME susceptibility (χ_{me}). Under frequency of 1MHz, tanδ of all samples is much less than 0.1 and essentially independent of H (as shown in fig. 6d). According to the simplified condition discussed by Jang et al.,[53] χ_{me} can be calculated by following expression:

$$[\varepsilon(H)-\varepsilon(0)]/\varepsilon(0)=(\chi_{me}/E_0)H$$

Where E_0 is the applied excitation signal 2.5V and H is the magnetic field. After considering the thickness of sample (0.56mm), we obtain that χ_{me} of D-$B_{0.57}C_{0.43}$ is about 0.16mV·cm^{-1}·Oe^{-1} at 2638Oe or 210038A·m^{-1}, which is larger than that of I-$B_{0.57}C_{0.43}$. But for $B_{0.8}C_{0.2}$ and $B_{0.67}C_{0.33}$ cases, MD effects in I-group samples are a slightly higher at the frequency of 1 MHz. These indicate the complexity of ME coupling: it is not only affected by the grain size and interfacial connection, but also influenced by the composition of ME composites.

From above measurements, $BaTiO_3$-$CoFe_2O_4$ composites synthesized by the simplified one pot solid-state reaction show

smaller grain sizes, tighter interfacial connection. Only talking about the magnetic or piezoelectric properties, D-group is not as good as I-group. But the strong interaction between two phases can bring better MD coupling in D-group. Our method provides a simple and new way to improve strain transfer. Just alike the double-edged sword, the strong interaction is bad from one side (magnetic/piezoelectric properties), but good from another side. Clear, higher ME effect inside a composite requires three essentials: high magnetostrictive, good piezoelectric properties from each individual functional phase, and strong interaction between them. If we cannot simultaneously achieve the maximum values for all three essentials, we would better to search an optimum combination of them.

4 Conclusions

Our results demonstrate that $BaTiO_3$-$CoFe_2O_4$ multiferroic composites fabricated by a simplified one pot solid-state reaction have smaller grain sizes, tighter interfacial connection, and enhanced MD effect than those obtained via the conventional two steps solid-state reaction. Due to the direct mixing and homogeneous distribution of all four basic chemicals (self-assemble to form two phases via reaction), different phases will block each other's growth, leading to relatively small grain size and much tighter interfacial connection. The tighter interfacial connection provides convenience to the strain transferring from the piezoelectric phase to magnetostrictive one (or in reverse). Better strain transfer will enhance the MD coupling in composites, indirectly benefiting the ME performance.

Acknowledgements

The authors gratefully acknowledge Ms. Yanzhu Dai from International Center for Dielectric Research at Xi'an Jiaotong University for her help to take SEM images. This work was supported by the Ministry of Science and Technology of China through a 973-Project under Grant No. 2012CB619401, National Natural Science Foundation of China (Grant No. 11204233), the Fundamental Research Funds for the Central Universities and the Scientific Research Foundation for the Returned Overseas Chinese Scholars, Ministry of Education.

Notes and references

1. N. Hur, S. Park, P. A. Sharma, J. S. Ahn, S. Guha and S. W. Cheong, *Nature*, 2004, 429, 392-395.
2. W. Eerenstein, M. Wiora, J. L. Prieto, J. F. Scott and N. D. Mathur, *Nature Materials*, 2007, 6, 348-351.
3. M. Gajek, M. Bibes, S. Fusil, K. Bouzehouane, J. Fontcuberta, A. Barthelemy and A. Fert, *Nat Mater*, 2007, 6, 296-302.
4. Y. H. Chu, L. W. Martin, M. B. Holcomb, M. Gajek, S. J. Han, Q. He, N. Balke, C. H. Yang, D. Lee, W. Hu, Q. Zhan, P. L. Yang, A. Fraile-Rodriguez, A. Scholl, S. X. Wang and R. Ramesh, *Nat Mater*, 2008, 7, 478-482.
5. L. W. Martin, S. P. Crane, Y. H. Chu, M. B. Holcomb, M. Gajek, M. Huijben, C. H. Yang, N. Balke and R. Ramesh, *Journal of Physics: Condensed Matter*, 2008, 20, 434220.
6. S. H. Baek, H. W. Jang, C. M. Folkman, Y. L. Li, B. Winchester, J. X. Zhang, Q. He, Y. H. Chu, C. T. Nelson, M. S. Rzchowski, X. Q. Pan, R. Ramesh, L. Q. Chen and C. B. Eom, *Nature Materials*, 2010, 9, 309-314.
7. J.F.Scott, *Journal of Materials Chemistry*, 2012, 22, 4567-4574.
8. N. Ce-Wen, M. I. Bichurin, D. Shuxiang, D. Viehland and G. Srinivasan, *Journal of Applied Physics*, 2008, 103, 031101.
9. N. A. Hill, *J.Phys.Chem.B*, 2000, 104, 6694-6709.
10. W. Eerenstein, N. D. Mathur and J. F. Scott, *Nature*, 2006, 442, 759-765.
11. S.-W. C. M. Mostovoy, *Nature Materials* 2007, 6, 13-20.
12. E. Ascher, *Journal of Applied Physics*, 1966, 37, 1404.
13. N. A. Spaldin, *Physical Review B*, 2005, 71.
14. C. A. Vaz, J. Hoffman, C. H. Ahn and R. Ramesh, *Adv Mater*, 2010, 22, 2900.
15. C. E. N. A. Spaldin, *Physical Review Letters*, 2005, 95.
16. J. L. MacManus-Driscoll, *Advanced Functional Materials*, 2010, 20, 2035-2045.
17. G. Caruntu, A. Yourdkhani, M. Vopsaroiu and G. Srinivasan, *Nanoscale*, 2012, 4, 3218-3227.
18. Y. Yang, S. Priya, Y. U. Wang, J.-F. Li and D. Viehland, *Journal of Materials Chemistry*, 2009, 19, 4998.
19. Z. Jian-ping, H. Hongcai, S. Zhan and N. Ce-Wen, *Applied Physics Letters*, 2006, 88, 013111.
20. H. Zheng, J. Wang, S. E. Lofland, Z. Ma, L. Mohaddes-Ardabili, T. Zhao, L. Salamanca-Riba, S. R. Shinde, S. B. Ogale, F. Bai, D. Viehland, Y. Jia, D. G. Schlom, M. Wuttig, A. Roytburd and R. Ramesh, *Science*, 2004, 303, 661.
21. S. Xie, F. Ma, Y. Liu and J. Li, *Nanoscale*, 2011, 3, 3152.
22. R. R. N. A. SPALDIN, *Nature Materials*, 2007, 6, 21-29.
23. J. Ma, J. Hu, Z. Li and C. W. Nan, *Adv Mater*, 2011, 23, 1062-1087.
24. N. Bassiri-Gharb, Y. Bastani and A. Bernal, *Chem Soc Rev*, 2013, 10, 1039.
25. D. R. T. A.M.J.G. Run, and J.H. Scholing *Journal of Materials Science*, 1974, 9, 1710.
26. J. Vandenbo., D. R. Terrell, R. A. J. Born and H. Giller, *Journal of Materials Science*, 1974, 9, 1705.
27. R. A. J. b. J. vanden boomgaard, *Journal of Materials Science*, 1978, 13, 1538.
28. I. Kagomiya, Y. Hayashi, K.-i. Kakimoto and K. Kobayashi, *Journal of Magnetism and Magnetic Materials*, 2012, 324, 2368-2372.
29. W. C. Vittayakorn, N. Pulphol, R. Muanghlua and N. Vittayakorn, *Integrated Ferroelectrics*, 2013, 148, 153-160.
30. C. M. Kanamadi, B. K. Das, C. W. Kim, D. I. Kang, H. G. Cha, E. S. Ji, A. P. Jadhav, B. E. Jun, J. H. Jeong, B. C. Choi, B. K. Chougule and Y. S. Kang, *Materials Chemistry and Physics*, 2009, 116, 6-10.
31. L. M. Hrib and O. F. Caltun, *Journal of Alloys and Compounds*, 2011, 509, 6644-6648.
32. R. Rani, J. K. Juneja, S. Singh, C. Prakash and K. K. Raina, *Journal of Magnetism and Magnetic Materials*, 2013, 345, 55-59.
33. C. Schmitz-Antoniak, D. Schmitz, P. Borisov, F. M. de Groot, S. Stienen, A. Warland, B. Krumme, R. Feyerherm, E. Dudzik, W. Kleemann and H. Wende, *Nat Commun*, 2013, 4, 2051.
34. H. Zheng, F. Straub, Q. Zhan, P. L. Yang, W. K. Hsieh, F. Zavaliche, Y. H. Chu, U. Dahmen and R. Ramesh, *Advanced Materials*, 2006, 18, 2747-2752.
35. I. Levin, J. Li, J. Slutsker and A. L. Roytburd, *Advanced Materials*, 2006, 18, 2044-2047.
36. X. L. Lu, Y. Kim, S. Goetze, X. G. Li, S. N. Dong, P. Werner, M. Alexe and D. Hesse, *Nano Letters*, 2011, 11, 3202.
37. D. Chaoyong, Z. Yi, M. Jing, L. Yuanhua and N. Ce-Wen, *Acta Materialia*, 2008, 56, 405.
38. M. Lorenz, M. Ziese, G. Wagner, J. Lenzner, C. Kranert, K. Brachwitz, H. Hochmuth, P. Esquinazi and M. Grundmann, *CrystEngComm*, 2012, 14, 6477.
39. M. Etier, V. V. Shvartsman, Y. Gao, J. Landers, H. Wende and D. C. Lupascu, *Ferroelectrics*, 2013, 448, 77-85.
40. V. Corral-Flores, D. Bueno-Baqués and R. F. Ziolo, *Acta Materialia*, 2010, 58, 764-769.
41. R. G. Giap V. Duong, Reiko Sato Turtelli, *IEEE Transactions on Magnetics*, 2006, 42.
42. V. Corral-Flores, D. Bueno-Baques and R. F. Ziolo, *Acta Materialia*, 2010, 58, 764-769.
43. V. V. Shvartsman, F. Alawneh, P. Borisov, D. Kozodaev and D. C. Lupascu, *Smart Materials & Structures*, 2011, 20.
44. S. H. Xie, J. Y. Li, Y. Qiao, Y. Y. Liu, L. N. Lan, Y. C. Zhou and S. T. Tan, *Applied Physics Letters*, 2008, 92.

45. L. Bin, W. Chunqing, Z. Wei, H. Chunjin, F. Jingming and W. Hong, *Materials Letters*, 2013, 91, 55-58.
46. J. P. Velev, S. S. Jaswal and E. Y. Tsymbal, *Philos Trans A Math Phys Eng Sci*, 2011, 369, 3069-3097.
47. J. D. Burton and E. Y. Tsymbal, *Philos Trans A Math Phys Eng Sci*, 2012, 370, 4840-4855.
48. Y. Yang, S. Priya, J.-F. Li and D. Viehland, *Journal of the American Ceramic Society*, 2009, 92, 1552.
49. J. Van Suchtelen, *Philips Res. Rep*, 1972, 27, 28-37.
50. K. K. P. R P Mahajan, M B Kothale, S C Chaudhari, V L Mathel and S A Patil, *Pramana-journal of physics*, 2002, 58.
51. G. V. Duong and R. Groessinger, *Journal of Magnetism and Magnetic Materials*, 2007, 316, e624-e627.
52. Y. Liu, X. Ruan, B. Zhu, S. Chen, Z. Lu, J. Shi and R. Xiong, *Journal of the American Ceramic Society*, 2011, 94, 1695-1697.
53. H. M. Jang, J. H. Park, S. Ryu and S. R. Shannigrahi, *Applied Physics Letters*, 2008, 93, 252904.
54. M. P. Singh, W. Prellier, C. Simon and B. Raveau, *Applied Physics Letters*, 2005, 87.
55. I. Fina, N. Dix, L. Fàbrega, F. Sánchez and J. Fontcuberta, *Thin Solid Films*, 2010, 518, 4634-4636.
56. G.Catalan, *Applied Physics Letters*, 2006, 88.